A comparative study of Machine Learning and Deep Learning methods for flood forecasting in the Far-North region, Cameroon

Francis Yongwa Dtissibe, Ado Adamou Abba Ari, Alidou Mohamadou, Hamadjam Abboubakar, Arouna Ndam Njoya, Ousmane Thiare

Scientific African 23 (2024) e02053

Contents lists available at ScienceDirect

Scientific African

journal homepage: www.elsevier.com/locate/sciaf

A comparative study of Machine Learning and Deep Learning methods for flood forecasting in the Far-North region, Cameroon

Francis Yongwa Dtissibe [a], Ado Adamou Abba Ari [a,b,c,*], Hamadjam Abboubakar [d], Arouna Ndam Njoya [d], Alidou Mohamadou [a], Ousmane Thiare [e]

[a] LaRI Lab, University of Maroua, PO Box 814, Maroua, Cameroon
[b] DAVID Lab, Université Paris Saclay, University of Versailles Saint-Quentin-en-Yvelines, 45 Avenue des États-Unis 78035 Versailles cedex, France
[c] CREATIVE, Institute of Fine Arts and Innovation, University of Garoua, PO Box 346, Garoua, Cameroon
[d] Department of Computer Engineering, University Institute of Technology, University of Ngaoundéré, PO Box 455, Ngaoundéré, Cameroon
[e] Department of Computer Science, Gaston Berger University, PO Box 234, Saint-Louis, Senegal

ARTICLE INFO

Editor name: Ahmed Kenawy

Keywords:
Machine Learning
Deep Learning
Short-term
Long-term
Flood
Forecasting
Comparison
Performance
Far-North
Cameroon
Resilience

ABSTRACT

Flood crises are the consequence of climate change and global warming, which lead to an increase in the frequency and intensity of heavy rainfall. Floods are, and remain, natural disasters that result in huge loss of lives and material damage. Flood risks threaten all countries of the globe in general. The Far-North region of Cameroon has suffered of flood crises on several occasions, resulting in significant loss of human lives, infrastructural and socio-economic damage, with the destruction of homes, crops and grazing areas, and the halting of economic activities. The models used for flood forecasting in this region are generally physical-based, and produce unsatisfactory results. The use of artificial intelligence based methods for flood forecasting in order to limit its consequences is a way to be explored in the Far-North region of Cameroon. The aims of the present research work is to design and compare the performance of Machine Learning and Deep Learning based models such as one dimensional Convolutional Neural Network, Long and Short Term Memory and Multi Layer Perceptron for short-term and long-term flood forecasting in the Far-North region of Cameroon. The models designed take as input the temperature and rainfall time series recorded in this region. Performance criteria used for evaluating models are Nash–Sutcliffe Efficiency, Percent Bias, Coefficient of Determination and Root Mean Squared Error. As the results of the design and performance comparison of the models, the best model for short-term flood forecasting is the LSTM model , and the best model for long-term flood forecasting is still the LSTM model. The best models obtained from the comparisons have satisfactory performance and good generalization capabilities, as reflected by the performance criteria. The results of our research work can be used for implementation of floods warning systems and for definition of an effective and efficient flood risk management policies in order to make the Far-North region of Cameroon more resilient to flood crises.

Introduction

Since the 1960s, floods remain the most frequent climatological disasters, and its proportion is steadily increasing [1]. In the same ways, 45.54% of natural disasters were floods in the last ten years [1]. According to [2–4], floods are the most frequent among natural disaster and they can occur anywhere after heavy rainfall, causing a huge loss of lives and material damage. Floods disasters

* Corresponding author at: CREATIVE, Institute of Fine Arts and Innovation, University of Garoua, PO Box 346, Garoua, Cameroon.
E-mail address: adoadamou.abbaari@gmail.com (A.A.A. Ari).

https://doi.org/10.1016/j.sciaf.2023.e02053
Received 2 September 2023; Received in revised form 19 December 2023; Accepted 21 December 2023
Available online 27 December 2023

have increased, causing economic destabilization, social devastation, infrastructure destruction, and environmental erosion and collapse, especially in indigenous communities [5]. The severity of floods is most visible in a country where structural accessibility is insufficient due to limited financial resources [6]. The consequences of extreme meteorological events is greater in Africa than in other regions of the world due to Africa's low adaptive capacity, high reliance on ecosystem resources for livelihoods and climate-sensitive agriculture [7]. The authors in [6] have noticed that the number of households displaced and made homeless by floods is increasing dramatically in Africa.

Maga and neighborhoods in Cameroon's Far-North region has been the scene of flood crises, in August and September 2012, 30,000 people were affected with huge material and infrastructural damage, deterioration of economic, social, crop and livestock activities [8]. Cameroon's Far-North region has been again, in 2020, affected by floods due to heavy rainfall with similar consequences. The authors in [9] carried out morphological, pedological and climatic studies for the mapping of flood risk areas in Maga and its surroundings in Cameroon's Far-North region, and they found that the conditions which favor flooding include impermeable soils, low vegetation cover and heavy rainfall concentrated over four months. The authors in [10] used traditional methods for precipitation trends and flood risks study in Cameroon's Far-North region. Thirty of the forty municipalities in the Cameroon's Far-North region have been affected at least once by floods according to the analyses of the history of flood disasters carried out by [10].

The consequences of floods are numerous: loss of lives, livelihoods, material damage, extensive direct and indirect health impacts, discouragement of public and private investment [1]. The reduction of exposure and losses of lives, material and infrastructural damage is the aim of flood risk management strategies [11]. According to [12], flood risk management can be achieved by implementing legal, economic, political, educational, structural, technological, cultural, social, health, environmental, and institutional measures to reduce and prevent hazard, vulnerability, and exposure. The most effective way to handle disasters is to prevent them from happening in the first place [13]. To reduce these consequences, several flood forecasting methods are used such as: conceptual, empirical, physical based and probabilistic methods [6]. The methods used for rainfall forecasting were based on hydrodynamic theories before the 1990s [14]. Numerical models gradually came to prominence along with the rapid development of computers after the 1900s, and technologies based on Artificial Intelligence (AI) have developed at an exponential speed, and have rapidly emerged in the field of meteorology [14].

For [12], in areas with no data or few data, several methods can be used to estimate peak flows and the return period of floods. Since it is very difficult to measure hydrological variables in real time due to the lack of ground-based meteorological stations in a poor country, Machine Learning (ML), which learns from few observed data, is more reliable for hydrological forecasting [6]. ML and Deep Learning (DL) based methods have been shown to be promising for flood modeling and offer a useful alternative to physical-based hydraulic models, which are computationally demanding and difficult to use in operational flood forecasting systems [15]. In this light, ML and DL methods can be combined with traditional methods to improve their performance. The authors in [16] proposed an adjustment module based on learning methods, which uses forecast data from hydraulic models to give dynamic auto-adaptation capability to flood forecasting systems.

The methodology used to carry out our research consists of the following steps: data collection and preprocessing, model design and training, model testing and performance evaluation, model performance comparison, and selection of the best performing models. The structure of our research work is organized as follows. Some related works are presented in Section "Related works". The ML and DL techniques used for the design of short- and long-term floods forecasting models are presented in Section "ML and DL models" of this research work. Section "Study area and data" presents the study area and the data used in this research work. The methodology used for the design and comparison of the different models, the performance evaluation criteria and the tests of these models are presented in Section "Design and comparison of models". Section "Results and discussion" presents the results and the discussions of this research work. Conclusion of our research work is made in Section "Conclusion".

Related works

As applications of data-driven, AI models such as Adaptive Neuro-Fuzzy Inference System (ANFIS), Artificial Neural Network (ANN), Genetic Programming (GP), Multi-Layer Perceptron (MLP), Support Vector Machine (SVM), and DL algorithms find their place in the field of hydrology [17]. Application of ML tools such as ANN, SVM and several prediction systems to flood forecasting appear to be more efficient than physical-based methods [18].

Many more studies on performance comparison of ML and DL models for flood forecasting have been conducted by several authors (Table 1). The authors in [20] worked on comparison of LSTM and 1D-CNN models for real-time flood forecasting in Red River of the North of United State of America (USA) using streamflow data. The results of the study shown that the LSTM model is the best performed. The authors in [19] compared ML and DL models for water level forecasting of Surma River at Sylhet city using daily discharge and water level data. The Exponential Gaussian Process Regression Model showed the best performance than others models. Compared ML and DL models had better performance than the MIKE-11 in term of R^2 for 2, 4, and 5 days lead time. The authors in [33] carried out study on improving flood forecasting using DL techniques for the banks of river Daya and Bhargavi that flows across Odisha in India. They compared the Deep Belief Network with Teaching Learning-Based Optimization method. In this study, floods were forecasted 1 day, 1 week and 2 weeks ahead. The authors in [22] carried out study on stacked ML algorithms and Bidirectional LSTM (Bi-LSTM) for multistep ahead streamflow forecasting. Models were used for daily prediction of streamflow of the Bacchiglione River, the Raccoon River, the Wilson River, and the Trent River. The both models used had very high accuracy in several cases; therefore, stacked models perform better than Bi-LSTM model for peak prediction in many cases. The authors in [21] worked on improving multistep ahead prediction ability for long-term streamflow forecasting in a poorly

Table 1
Performance comparison of ML and DL techniques for flood forecasting.

Ref.	Modeling techniques compared	Input variables	Output variables	Prediction type	Best model	Region
[19]	EGPR, Bagged Trees, MIKE-11,	Discharge, Water level	Water level	Daily	EGPR	Bangladesh
[20]	LSTM, 1D-CNN	Streamflow	Streamflow	Real-time	LSTM	USA
[21]	3D-CNN-T, TD-CNN-T, TD-CNN-LSTNet, 3D-CNN-LSTNet	Streamflow	Streamflow	Long-term	3D-CNN-T	Persian Gulf
[22]	Stacked ML algorithms, Bi-LSTM	Streamflow	Streamflow	Daily	Stacked ML algorithms	Italy, New Zealand, USA
[23]	FFNN, CNN, LSTM	Streamflow	Streamflow	Daily	LSTM	Vietnam
[24]	WASH123D, HEC-HMS, SVM	Radar rainfall	Flood level	Hourly	SVM for QPF	Taiwan
[25]	LR, MLP, SVM, LSTM	Precipitation, Streamflow	Streamflow	Daily	LSTM	USA
[26]	CNN, RNN, KNN, MLP, SVM, DT, RF, LR	Temperature, Rainfall intensity	Flood	Monthly	CNN, KNN	Iraq
[27]	ANN, SVR, DT, RFA, LSTM	Rainfall	Rainfall	Weekly	LSTM	Malaysia
[28]	ANFIS, SVM, GEP	18 parameters	Flood discharge	Long-term	ANFIS, SVM, GEP	Iran
[29]	MLR, MLP, ANFIS	Climate signals	Precipitation (SPI)	Long-term	MLP	Iran
[30]	AR, ANN, ANFIS	Reservoir inflow	Reservoir inflow	Monthly	ANFIS	India
[31]	ARMA, ANN, ANFIS, GP, SVM	River flow discharge	River flow discharge	Monthly	ANFIS, GP, SVM	Asia
[32]	ANFIS, ANN, GRNN, FFNN, AR	River flow, Rainfall	River flow	Daily	ANFIS	Turkey

gauged basin. They used geo-spatiotemporal mesoscale data and attention-based DL. They compared models for 12-months ahead prediction using monthly historical records of streamflow of the Karkheh River basin in the northeast of the Persian Gulf. The results shown that the 3D-CNN-Transformer was the best performed model, followed by the TimeDistributed-CNN-Transformer (TD-CNN-Transformer), TimeDistributed-CNN-Long- and Short-term Time-series network (TD-CNN-LSTNet), and 3D-CNN-LSTNet. The authors in [24] worked on comparative study of very short term flood forecasting using a data-driven prediction model and physical-based numerical models. Their objective was to compare the performances of physical-based models WASH123D (Watershed model of various spatial–temporal scales) and HEC-HMS (Hydrologic Engineering Center-Hydrologic Modeling System), and the SVM model for hourly flood level forecasting in the Fengshan Creek basin of Northern Taiwan, using radar rainfall data. The results show that the SVM model is an interesting solution to improve the accuracy of Quantitative Precipitation Forecasts (QPF) forecasted flood levels. The authors in [23] compared some DL techniques for river streamflow forecasting in Red River basin of the north of Vietnam using daily runoff data. FeedForward Neural Network (FFNN), CNN and LSTM-based models were compared in this study. Streamflow were forecasted for one and two days ahead. As the results of the study, LSTM-based models perform better than FFNN and CNN models. The authors in [25] worked on comparison between LSTM-based model and conventional Machine Learning algorithms for streamflow forecasting. The aim of this work was to compare the accuracy of some data-driven models, Linear Regression (LR), LSTM, MLP, and SVM on daily streamflow forecasting. Input data used were rainfall and streamflow time series of the Kentucky River basin in Eastern Kentucky of US. The results indicate that the LSTM model is the best in daily streamflow forecasting. The authors in [26] did a comparative study on some selected models (DL, ML, and SVM) for flood forecasting in Eastern Iraq. In this study, temperature and rainfall intensity were used to compare performance of CNN, Recurrent Neural Network (RNN), MLP, SVM, K-Nearest Neighbor (KNN), Decision Tree (DT), Random Forest (RF), and LR on predicting the occurrence of flood. The results show that CNN and KNN models outperformed the other flood forecasting models. The authors in [27] worked on comparing ML models for rainfall forecasting. Five ML models ANN, Support Vector Regression (SVR), DT, Random Forest Algorithm (RFA), and LSTM were compared using weekly average rainfall data from Kuala Krai rainfall stations, Malaysia. The results show that the best performing model is LSTM model. The authors in [28] worked on comparison of several data-driven models such as ANFIS, SVM, and GP for regional flood frequency modeling in West Iran. Eighteen parameters were used as input variable for compared models. The results indicate that the three models have good performances. The authors in [29] applied Multiple Linear Regressions (MLR), MLP, and ANFIS for precipitation forecasting based on largescale climate signals. Climate signals were calculated from precipitation data of meteorological stations of Maharlu-Bakhtaram catchment, and were used as input variable of models. Performance comparison of models shows that MLP model is the best in precipitation (SPI) forecasting. The authors in [30] worked on comparison between adaptive neuro-fuzzy, autoregressive, and neural network models for hydrological time series modeling. The performances of different models were compared using monthly reservoir inflow data of Sutlej river. The results of the work indicate that the ANFIS model has the best performance for monthly reservoir inflow forecasting. The authors in [31] worked on

performance comparison of several AI techniques for forecasting monthly discharge time series. Monthly river flow discharge data of Manwan Hydropower in Lancangjiang River and Hongjiadu Hydropower on Wujiang River were used for performance comparison of ANFIS, ANN, Auto Regressive Moving Average (ARMA), GP, and SVM models. The results show that ANFIS, GP and SVM models have the best performance. The authors in [32] worked on comparison of artificial intelligence techniques for river flow forecasting. In this study, the performances of five ML models ANFIS, ANN, Generalized Regression Neural Network (GRNN), FFNN, and Auto Regressive (AR) are compared using daily river flow and rainfall data of River Seyhan and River Cine, Turkey. The results indicate that the ANFIS model is the best for daily river flow forecasting.

Several research works have been conducted on the use of CNNs for flood modeling. Precisely, [34] used Deep neural networks for rainfall estimation from remotely sensed data; [35] used 1D Deep CNN for Rainfall Forecasting; [36] carried out research on deep CNN model for rapid forecasting of fluvial flood inundation; [37] modeled rainfall-runoff using CNN techniques; [38] used CNN for forecasting flood in Internet of Things (IoT) enabled smart city; [39] applied 1D Convolutional Neural Networks for Daily Rainfall Prediction; [40] used DL technique for forecasting hydrological time-series. LSTM is appropriate for modeling time series with long-term dependencies [41]. In fact, numerous studies exist, including that on flood forecasting using time series and LSTM conduced by [42]. Similarly, [43] applied LSTM model for flood forecasting. The authors in [44] used LSTM network for flash flood forecasting, and [41,45,46] used them for rainfall-runoff modeling, [47] used a LSTM model to carry out the forecasting of summertime seasonal-scale rainfall, [48] worked on multi-step-ahead flood forecasting using a LSTM-based Encoder–Decoder framework, [49] carried out work on forecasting short-term household load using LSTM time series model. The authors in [50] used LSTM for forecasting flood susceptibility. The authors in [51] used a LSTM model to boost river streamflow forecasts over the western US. The use of ML tools such as neural networks can significantly increase the performance of weather forecasting systems [52]. The usage of Artificial Neural Network as a hydrologic forecasting technique to improve the accuracy of flood forecasts in hydrological modeling domains has a primordial role in flood risk management strategies [6]. Artificial Neural Networks are widely used ML techniques for designing flood forecasting models [2,6,53–63].

The various studies carried out on flood forecasting using ML and DL techniques show that a multitude of techniques can be used for flood forecasting. The input data used, the forecast horizons, the output variables and the areas of application are varied. The results of these studies highlight the fact that the best models are only known at the end of the comparison, and that none of their characteristics allow us to say in advance that they will be better than the others. It is therefore necessary to proceed by experimentation to compare and determine the best models based on the input data and output variables, the forecast horizon, and the dataset dimension.

ML and DL models

1D-CNN

The CNN is a deep neural network with several hidden layers that simulates the functioning of the visual cortex of the brain in order to recognize and classify objects or images, and detect an object in an image [64]. They are mainly used for image processing and pattern recognition. The weight sharing concept is the main difference between CNN and MLP [65]. Three types of CNN are found in literature: 1D-CNN, 2D-CNN and 3D-CNN. The authors in [65] described Conv1D as follows: In one-dimensional CNN, the convolution kernels move in one direction. The input and output data of Conv1D are two-dimensional. Conv1D is mainly used for time series data and has a powerful feature extraction capability: the nonlinear features hidden in the raw data can be automatically extracted by the alternating convolution layer and the pooling layer in Conv1D, and adaptive feature learning is completed in the fully-connected layer. In this way, the Conv1D algorithm eliminates the manual feature extraction process in conventional algorithms and enables end-to-end information processing. Fig. 1 shows our Conv1D model. One of the main advantages of the CNN model is the ease of the training phase due to the reduced number of weights compared to a fully connected architecture. Convolutional layer and pooling layer are expressed by Eqs. (1) and (2) respectively [66].

$$g_i = f\left[\sum_{n=1}^{N} conv1D(w_{i,n}, a_n) + b_i\right] \tag{1}$$

where g_i is the result of the ith filter, a the input data of size $1 \times N_a \times N$, w_i the weight matrix of the ith filter, the size of which is $1 \times N_w \times N$, and b_i and f the bias of the ith filter and the activation function respectively.

$$p_i(j) = \max_{(j-1)\times m < k \le j \times m} (a_i(k)) \tag{2}$$

where $a_i(k)$ is the kth element of the ith feature map input into the pooling layer and $p_i(j)$ is the jth element of the ith feature map output by the pooling layer. The size of the pooling layer filter is $1 \times m$.

Several architectures of 1D-CNN models have been designed and trained. These architectures are obtained by alternating the conv1D and Maxpooling1D layers, then adding fully connected layers (1 to 3) and an output layer with a single neuron. For the conv1D layers, the input data size varies from (4,2) to $(30, 2)$, the number of filters used is 16, 32 and 64, the kernel size is 3 and the activation function used is ReLU function. The pool_size parameter for Maxpooling layers is 2. Dense layers (fully connected layers) varies between 32, 64 and 128, and their activation function is the ReLU function. The activation function of the output layer is

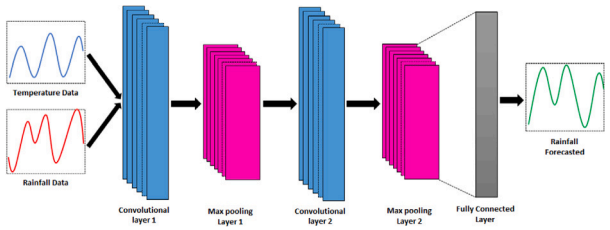

Fig. 1. Architecture of 1D-CNN model.

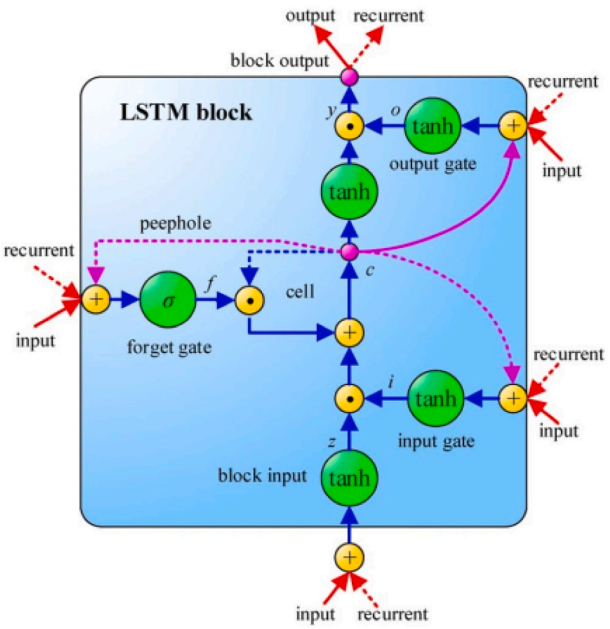

Fig. 2. LSTM memory block architecture [65].

the linear function. The optimization function used to train 1D-CNN models is the Adam function and the loss associated with this function is the MSE (Eq. (3)).

$$MSE = \frac{1}{n}\sum_{k=1}^{n}\left(y_k - y_k^p\right)^2 \tag{3}$$

where y_k is the observed rainfall at time k, and y_k^p the calculated rainfall at the same time k.

LSTM

LSTM models are designed to learn long-term dependencies in data and are able to overcome vanishing and exploding gradients problems of Recurrent Neural Network [25,65]. LSTM models have been introduced by authors in [67]. The architecture of LSTM consists of an input layer, one or more memory cells and an output layer [68]. The number of input variables is the same as the number of neurons in the input layer. Memory cells of LSTM models have three types of gate, input gate, forget gate and output gate. These gates are used to update and control the flow of data in the memory blocks [65]. Fig. 2 presents LSTM memory block architecture.

LSTM update equations are presented in [25,68,69]. These equations are given below (see Eqs. (4)–(10)):

$$g(t) = \tanh(W_{gx}x(t) + W_{gh}h(t-1) + b_g) \tag{4}$$

$$i(t) = \sigma(W_{ix}x(t) + W_{ih}h(t-1) + b_i) \tag{5}$$

$$f(t) = \sigma(W_{fx}x(t) + W_{fh}h(t-1) + b_f) \tag{6}$$

$$o(t) = \sigma(W_{ox}x(t) + W_{oh}h(t-1) + b_o) \tag{7}$$

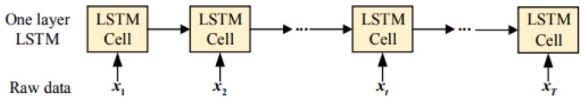

Fig. 3. Architecture of Vanilla LSTM model [70].

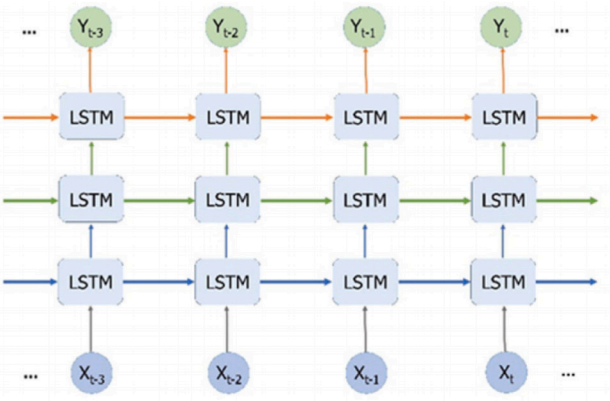

Fig. 4. Architecture of stacked LSTM model [23].

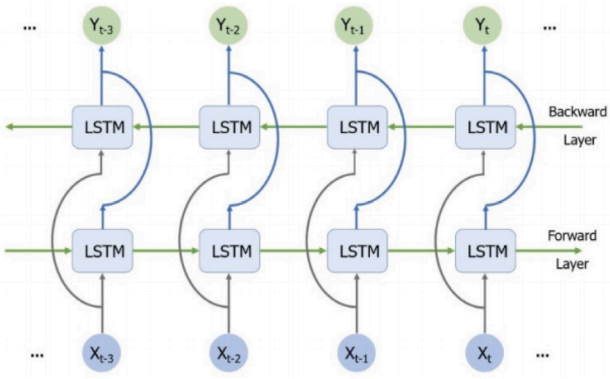

Fig. 5. Architecture of bidirectional LSTM model [23].

$$s(t) = g(t) \otimes i(t) + s(i-1) \otimes o(t) \tag{8}$$

$$h(t) = \tanh(s(t)) \otimes o(t) \tag{9}$$

$$y(t) = (W_{yh} h(t) + b_y) \tag{10}$$

where t is the current time, $x(t)$ the input vector, $g(t)$ input node, $i(t)$ input gate, $f(t)$ forget gate, $o(t)$ output gate, $s(t)$ cell state, $h(t)$ hidden state, W weights matrix, b bias vector, σ the sigmoidal function, tanh hyperbolic tangent function, $\otimes$ element wise multiplication, and $y(t)$ the output.

In our study, we designed and compared four LSTM-based models for short and long term flood forecasting: Bidirectional LSTM, Conv-LSTM, Stacked LSTM and Vanilla LSTM. The architectures of vanilla LSTM models consist of a single LSTM layer with a variable number of units (32, 50, 64 and 100) and a Dense layer consisting of a neuron (Fig. 3). The size of the input data is (number of samples, length of temporal window, number of features).

The architectures of stacked LSTM models are obtained by stacking several LSTM layers (2 to 5) made up of different numbers of units (32, 50, 64 and 100) and a Dense layer made up of a neuron (Fig. 4). The size of the input data is (number of samples, length of the temporal window, number of features).

The architectures of the Bi-LSTM models consist of several bidirectional layers (1 to 5) having different numbers of units (32, 50, 64 and 100)(Fig. 5). The size of the input data is (number of samples, length of temporal window, number of features).

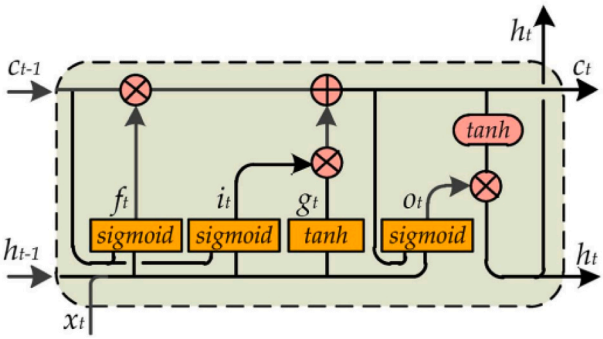

Fig. 6. Architecture of convLSTM model [71].

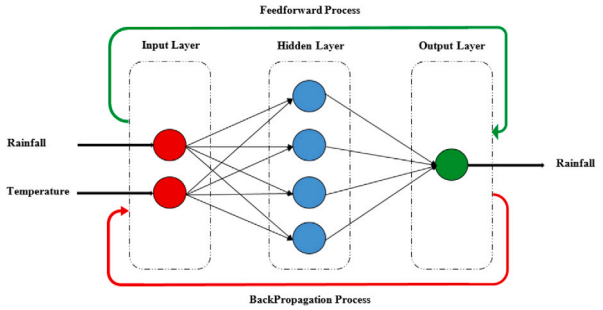

Fig. 7. Architecture of the MLP model.

The convLSTM model architectures are made up of several convLSTM2D layers (1 to 5) whose number of units varies (32, 50, 64 and 100) (Fig. 6). The kernel_size of the convLSTM layers is (3, 3). The number of filters varies between 32 and 64. A conv3D layer is added at the end of the model. The number of filters in this layer is 1, its kernel_size is $(3, 3, 3)$ and its activation function is the linear function. The input data size is (number of samples, time step,1, length of temporal window, number of features).

Number of samples and length of temporal window are parameters that vary, and therefore the architectures of LSTM models also vary according to these parameters. The linear function is used as the activation function for the neuron in the output layer of the different LSTM models. The optimization function used to train the LSTM models is the Adam function and the loss associated with this function is the MSE.

MLP

An ANN is a data-driven technique that focuses on data processing algorithm to solve a nonlinear problem [72]. MLP is a neural network with fully-connected architecture, which has the property of universal approximation [73,74] and parsimony [75] as well as the ability to approximate non-linear functions.

The architecture of our MLP model is as follows: an input layer (with the input variables rainfall and temperature), one hidden layer, and the output layer (with rainfall calculated by the model). Fig. 7 shows this architecture.

For a vector of input variables $x = [x_0, x_1, \ldots, x_n]$ and synaptic coefficients $w = [w_0, w_1, \ldots, w_n]$, the output y is given by the following expression (Eq. (11)):

$$y = f(g(x, w)) \tag{11}$$

where g is the aggregation function and f the activation function of the formal neuron. The aggregation function g used is the weighted sum given by Eq. (12) below:

$$g(x, w) = \sum_{i=0}^{n} x_i * w_i \tag{12}$$

We use the ReLU (Rectified Linear Unit) function as the activation function of the hidden layer neurons, and its expression is given by Eq. (13) :

$$f(y) = max(0, y) \tag{13}$$

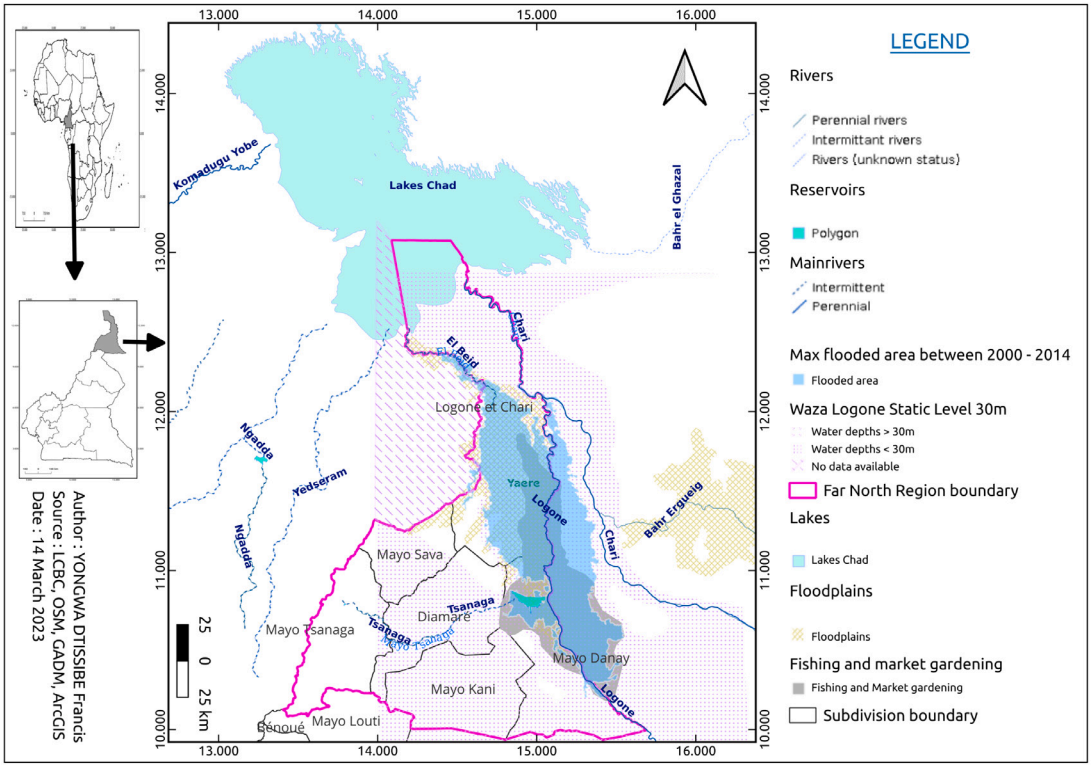

Fig. 8. Map of Cameroon's Far-North region.

The output y of the MLP model is calculated by the following relation (Eq. (14)):

$$y = w_{s,0} + \sum_{j=1}^{N_C} w_{s,j} f\left(w_{j,0} + \sum_{i=1}^{n} w_{j,i} x_i\right) \tag{14}$$

where x_i is the input variable of index i, N_C the number of neurons in the hidden layer, $w_{s,0}$ and $w_{j,0}$ the biases of neurons in the output and hidden layers, $w_{j,i}$ the synaptic coefficient linking the input variable of index i to the hidden neuron of index j, and $w_{s,j}$ the synaptic coefficient linking the hidden neuron of index j to the output neuron.

Several architectures of MLP models have been designed and trained. They are made up of the following layers and neurons: an input layer whose number of neurons varies from 4 to 30 (depending on the length of the temporal window), a hidden layer whose number of neurons varies from 3 to 20 [76,77] and an output layer made up of one neuron. The activation function for the neurons in the hidden layer is the ReLU function. The optimization function used to train the MLP models is the Adam function and the loss associated with this function is the MSE.

Study area and data

Study area

Cameroon's Far-North region is our study area. It is located between 10° and 13° North latitude, and 13°15 and 15°50 East longitude, and has an area of $34,263$ km^2. The area is the most populated region of Cameroon with about 3.5 million inhabitants and most exposed to climatic hazards [78,79]. It shares borders to the North with Lake Chad, to the South with the North region of Cameroon, to the East with the Republic of Chad, and to the West with the Federal Republic of Nigeria. The climate of the Far-North region is tropical with a Sahelian tendency, having a dry season of about 9 months, and a rainy season of about 3 months [10]. The highest temperatures are observed during the months of March and April; the lowest temperatures are recorded during the months of December, January and February. Rainfall in the region is relatively low, nevertheless falls very heavily over very short periods [9,79]. The main activities practiced by the population are agriculture, livestock and fishing [79,80]. The map of our study area is shown in Fig. 8.

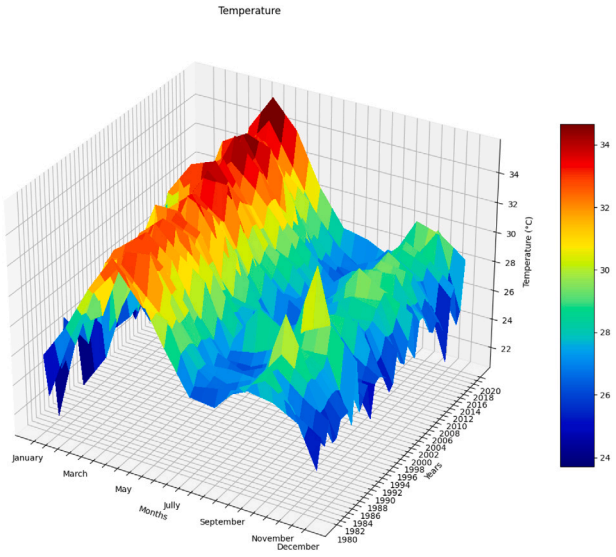

Fig. 9. 3D curves of temperature.

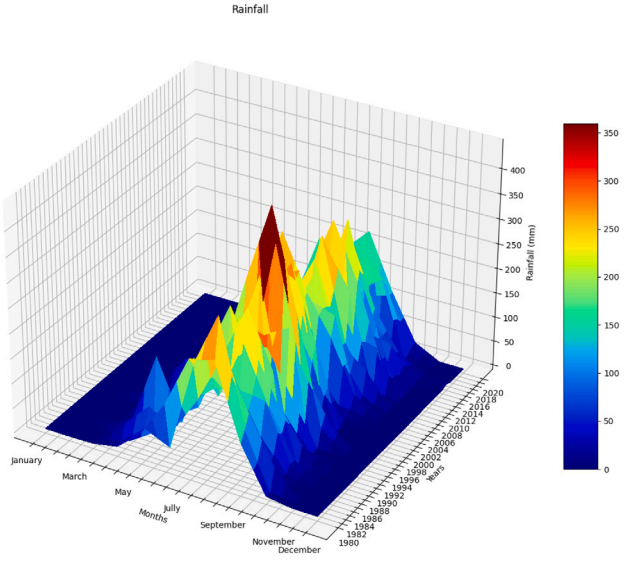

Fig. 10. 3D curves of rainfall.

Data and tools

The dataset used in our research are historical temperature and rainfall time series, which represent the input variables of our models. Thus, we have two features in our dataset. Temperature and rainfall time series were collected from meteorological measurement stations in the Far-North region of Cameroon. Temperatures and rainfall values are measured weekly or monthly from 1980 to 2020. The cumulative number of precipitation and temperature time series data points used in our work is $561,708,800$ points, or approximately 561.7 Mega data points. Our dataset has been split as follows: 80% of the dataset ($449,367,040$ data points) were used for models training and 20% of the dataset ($112,341,760$) were used for models testing. The curves of rainfall and temperature variations according to the years and months are shown in Figs. 9 and 10.

Rainfall is a very important input for hydrological models [81]. One of the consequences of climate change is the increase in rainfall and its frequency, which inevitably leads to flooding [82]. Similarly, the increase in temperature has an influence on the increase in rainfall according to the Clausius–Clapeyron thermodynamic theory [82]. Thus, temperature and rainfall are important variables for flood forecasting.

To carry out our study, we used Google Colaboratory plateform with Tensorflow and Keras for designing, training, testing and evaluating different ML and DL models.

Design and comparison of models

Methods

The analytical expression for the different flood forecasting models based on rainfall and temperature is given by Eq. (15).

$$Y(t+hp) = \varphi(R_{hp}(t), \ldots, R_{hp}(t-r_1+1), T_{hp}(t), \ldots, T_{hp}(t-r_2+1)) \tag{15}$$

where φ is the model's flood forecast function, Y calculated rainfall, R observed rainfall, T observed temperature, and r_1 and r_2 the time windows and hp the forecast horizon.

The steps used to carry out our research work are: data collection and preprocessing, model design and training, model testing and performance evaluation, model performance comparison, and selection of the best performing models.

The input data are rainfall and temperature time series. The preprocessing of the data consists in solving the problem of missing data, handling incorrectly coded values, performing data aggregation/interpolation and performing data normalization. The treatment of missing data was carried out using the simple arithmetic average method (Eq. (16)) described by [83].

$$V_o = \frac{\sum_{i=1}^{N} V_i}{N} \tag{16}$$

where V_o is the missing value to be estimated, V_i the value of the same parameter for the ith sample, and N the number of samples.

Data normalization is used in data preprocessing and improves the quality of prediction. The goal of data preprocessing is to minimize data noise, identify trends, and flatten the distribution of input variables [84]. Data normalization allows the data to fall within the interval $[0; 1]$, and avoid outliers. Eq. (17) below was used to perform the normalization.

$$X' = \frac{X - X_{min}}{X_{max} - X_{min}} \tag{17}$$

where X is the value to normalize, X' the new normalized value, X_{min} the minimum of the values to normalize, and X_{max} the maximum of the values to normalize.

For each type of forecast (short and long term), the models were trained and tested with rainfall and temperature time series data. Fig. 11 shows the flowchart of our methodology.

Model performance evaluation

The performance criteria used for model comparisons in our work are NSE (Nash–Sutcliffe Efficiency), $PBIAS$ (Percent Bias), R^2 (Coefficient of Determination), and $RMSE$ (Root Mean Squared Error).

The NSE is used for assessment of the correlation between the observed values and the values calculated by the models. NSE values close to 1 indicate good model performance. When the NSE value is equal to 1, then the observed values are equal to the values calculated by the model. The expression of the NSE is given by Eq. (18) below.

$$NSE = 1 - \frac{\sum_{k=1}^{n}\left(y_k - y_k^p\right)^2}{\sum_{k=1}^{n}\left(y_k - \overline{y}\right)^2} \tag{18}$$

where y_k is observed rainfall at time k, y_k^p calculated rainfall at time k, and $\overline{y}$ the average of the observed rainfall.

The $PBIAS$ is used to assess the quality of the model's training. It therefore allows us to check whether the model is underfitted or overfitted [85,86]. Eq. (19) expresses the $PBIAS$.

$$PBIAS(\%) = \left[\frac{\sum_{k=1}^{n}\left(y_k - y_k^p\right) * 100}{\sum_{k=1}^{n} y_k}\right] \tag{19}$$

where y_k is the observed rainfall at time k, and y_k^p the calculated rainfall at the same time k.

The coefficient of determination (R^2) assess the variance between the observed rainfall values and those calculated by the model. Its expression is given in Eq. (20) below.

$$R^2 = \frac{\sum_{k=1}^{n}\left(y_k - \overline{y}\right)\left(y_k^p - \overline{y^p}\right)}{\sqrt{\sum_{k=1}^{n}\left(y_k - \overline{y}\right)^2 \sum_{k=1}^{n}\left(y_k^p - \overline{y^p}\right)^2}} \tag{20}$$

where y_k is the observed rainfall at time k, $\overline{y}$ the average of observed rainfall, y_k^p the calculated rainfall at time k, and $\overline{y^p}$ the average of the calculated rainfall.

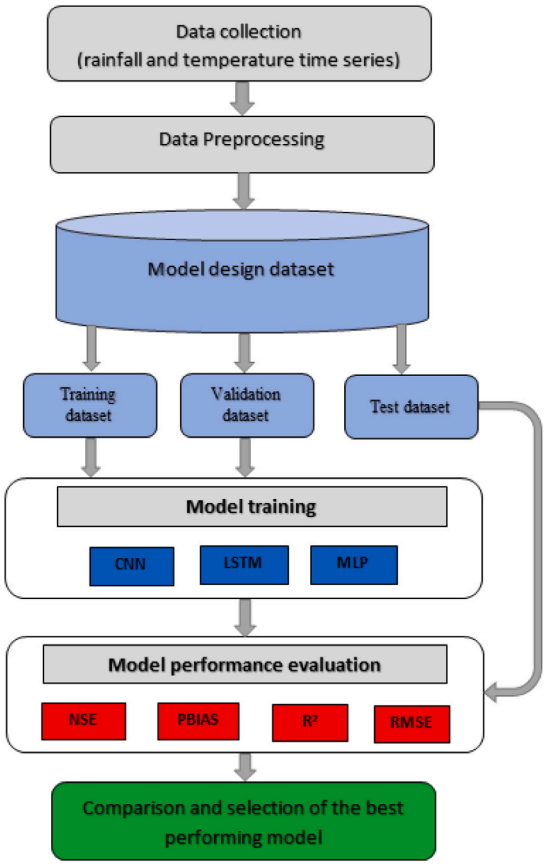

Fig. 11. Flowchart of the methodology.

Table 2
The goodness of fit [86,87].

S.N	Goodness of fit	NSE	$PBIAS$	R^2
1	Very good	$0.75 < NSE \leq 1$	$PBIAS < \pm 10$	$R^2 \geq 0.85$
2	Good	$0.65 < NSE \leq 0.75$	$\pm 10 \leq PBIAS < \pm 15$	$0.75 < R^2 \leq 0.85$
3	Satisfactory	$0.5 < NSE \leq 0.65$	$\pm 15 \leq PBIAS < \pm 25$	$0.60 < R^2 \leq 0.75$
4	Unsatisfactory	$NSE \leq 0.5$	$PBIAS \geq \pm 25$	$R^2 < 0.60$

The $RMSE$ determines the deviation of the forecast from the expected values. If the $RMSE$ is equal to 0, then the values obtained from the model are equal to the observed values. Its expression is given by Eq. (21):

$$RMSE = \sqrt{\frac{1}{n}\sum_{k=1}^{n}\left(y_k - y_k^p\right)^2} \tag{21}$$

where y_k is the observed rainfall at time k, and y_k^p the calculated rainfall at the same time k.

The acceptable NSE, $PBIAS$, and R^2 values of the hydrological models are presented in Table 2.

Results and discussion

The 1D-CNN, LSTM and MLP models were designed, trained and tested on rainfall and temperature time series data for short term flood forecasting with a time lag of 2. Table 3 shows the performance criteria (NSE, $PBIAS$, R^2 and $RMSE$) of the different models for short-term flood forecasting. The observed and calculated rainfall curves for test of these models are presented in Fig. 13. Fig. 12 represents the R^2 scatter plots of the models for training and test.

All the models were trained on the training dataset with a time lag of 22 for long term flood forecasting. The performance criteria of the different models for long-term flood forecasting are presented in Table 4. Fig. 15 shows the observed and calculated rainfall curves of the models for test. The R^2 scatter plots of the models for training and test are shown in Fig. 14.

Table 3
Models' performance criteria during training and test (short-term).

Models	Training				Testing			
	NSE	$PBIAS$	R^2	$RMSE$	NSE	$PBIAS$	R^2	$RMSE$
1D-CNN	0.93900	4.35361	0.96968	0.00655	0.90227	19.37708	0.96445	0.00608
LSTM	0.96945	1.06640	0.98490	0.00462	0.95118	4.74773	0.97631	0.00429
MLP	0.89496	7.40411	0.94886	0.00855	0.88108	1.10791	0.93894	0.00670

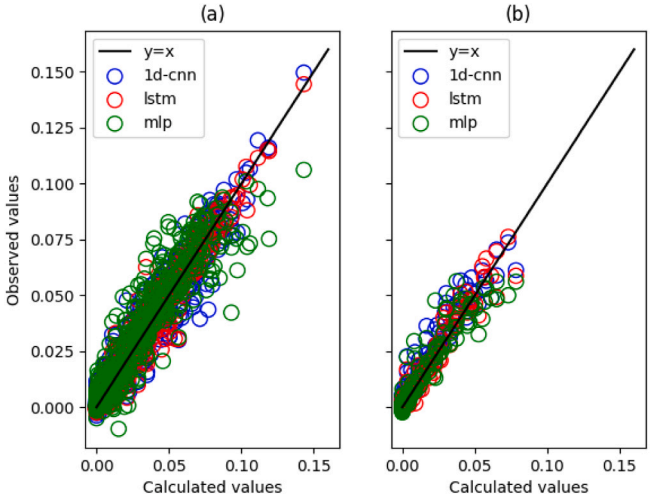

Fig. 12. Scatter plots of the models for training (a) and test (b).

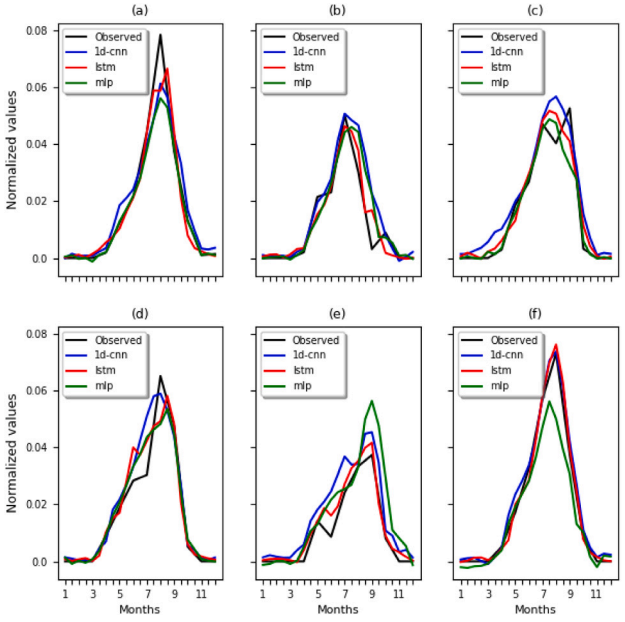

Fig. 13. Observed and calculated rainfall curves of models for test: 2015(a)–2020(f).

The comparison of the models for short-term flood forecasting shows that the best performing model is LSTM (Stacked) with the performance criteria presented in Table 5. According to Table 2 indicating the quality (goodness of fit) of the hydrological models according to the intervals of the values of the performance criteria, we can conclude that: for training, the $NSE = 0.96945$ is very

Table 4
Models' performance criteria during training and test (long-term).

Models	Training				Testing			
	NSE	$PBIAS$	R^2	$RMSE$	NSE	$PBIAS$	R^2	$RMSE$
1D-CNN	0.91624	4.18730	0.95789	0.00768	0.84693	4.19780	0.92137	0.00760
LSTM	0.94877	4.14095	0.97460	0.00599	0.92954	1.54409	0.96422	0.00516
MLP	0.86972	2.32371	0.93332	0.00958	0.81318	2.89724	0.90218	0.00840

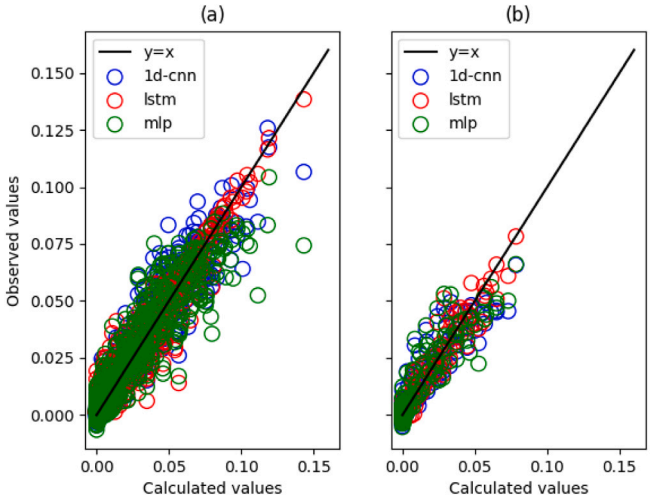

Fig. 14. Scatter plots of models for training (a) and test (b).

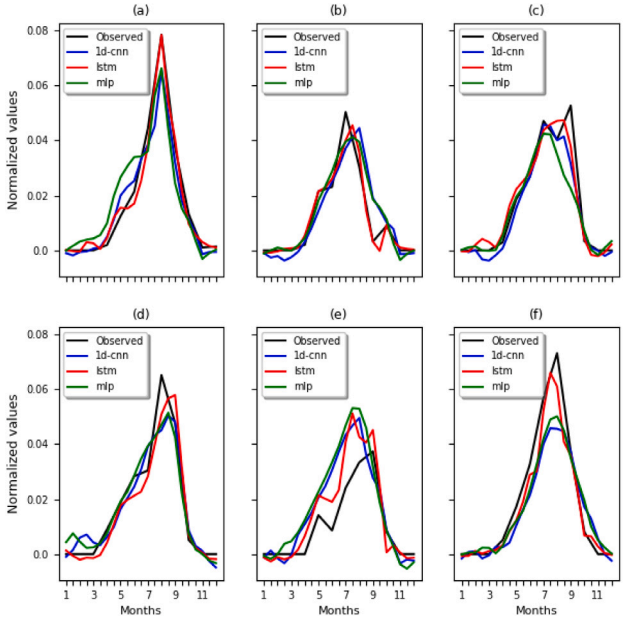

Fig. 15. Observed and calculated rainfall curves of models for test: 2015(a)–2020(f).

good, the $PBIAS = 1.06640$ very good, the $R^2 = 0.98490$ very good, and the $RMSE = 0.00462$ very good. For test of the LSTM model, the $NSE = 0.95118$ is very good, the $PBIAS = 4.74773$ very good, the $R^2 = 0.97631$ very good, and the $RMSE = 0.00429$ very good. The R^2 scatter plots for training and test of the best model are shown in Fig. 16. The observed and calculated rainfall curves of the best model for test are shown in Fig. 17.

For long-term flood forecasting, a comparison of the performance criteria of the different models shows that the best performing model is still LSTM (Stacked) model. Its performance criteria are presented in Table 6. The quality of the model according to the

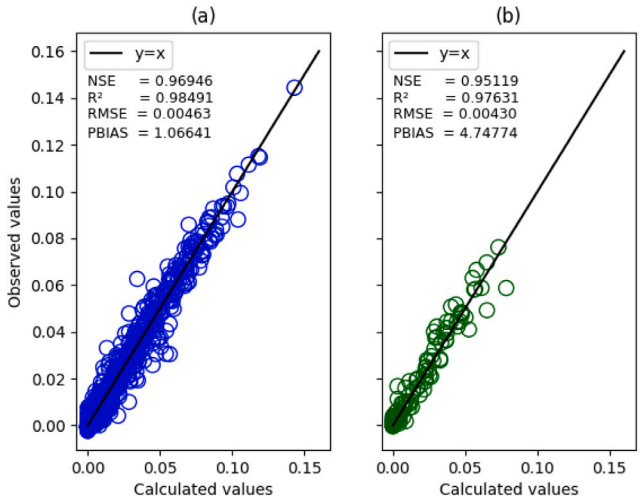

Fig. 16. Short-term forecasting — Scatter plots of the best model for training (a) and test (b).

Table 5
Performance criteria for the best model for short-term flood forecasting.

Model	Performance criteria	Training	Testing	Goodness of fit
LSTM	NSE	0.96945	0.95118	Very good
	$PBIAS$	1.06640	4.74773	Very good
	R^2	0.98490	0.97631	Very good
	$RMSE$	0.00462	0.00429	Very good

Table 6
Performance criteria for the best model for long-term flood forecasting.

Model	Performance criteria	Training	Testing	Goodness of fit
LSTM	NSE	0.94877	0.92954	Very good
	$PBIAS$	4.14095	1.54409	Very good
	R^2	0.97460	0.96422	Very good
	$RMSE$	0.00599	0.00516	Very good

values of the performance criteria shows that: for training, the $NSE = 0.94877$ is very good, the $PBIAS = 4.14095$ very good, the $R^2 = 0.97460$ very good, and the $RMSE = 0.00599$ very good. For test, the $NSE = 0.92954$ is very good, the $PBIAS = 1.54409$ very good, the $R^2 = 0.96422$ very good, and the $RMSE = 0.00516$ very good. The R^2 scatter plot for training and test of the best model are shown in Fig. 18. The observed and calculated rainfall curves of the best model for test are shown in Fig. 19.

The results of the tests show that the Stacked LSTM models for short and long term forecasting have very good flood forecasting performance. These models, therefore, have a good generalization capacity which reflects the absence of underfitting and overfitting during training according to the values of $PBIAS$. NSE values show a strong correlation between the calculated and observed values, which means that selected models perform well. Similarly, the R^2 and $RMSE$ values of selected models show small variation between the calculated and observed values. Therefore, the goodness of fit of ML and DL models (1D-CNN, LSTM and MLP) compared are in general good for both short and long term flood forecasts according to their performance criteria values. The training times of LSTM models are higher compared to other models. We have also observed that model performance decreases as the forecast horizon increases. More data is needed to improve model performance for longer forecast horizons. Our finding can be used to set up an automatic flood warning systems. They can also be used to implement flood risk management policies in the far north region of Cameroon. The ML and DL methods used in our research work can be applied in other regions with the same or other climatological features, but the results may differ from those obtained in our study.

Conclusion

Floods are the most frequent natural hazards causing a huge loss of human lives, material and economic damage all over the world. Cameroon's Far-North region has experienced several flood crises resulting in loss of lives, infrastructural damage and adverse consequences on socio-cultural activities practiced in the area. In view of the above, there is a need to adopt effective and efficient flood risk management policies. ML and DL methods for flood forecasting are alternatives to the less efficient traditional hydrological methods. The aim of this study was to design and compare the ML and DL methods for short and long term flood forecasting in the Far-North region of Cameroon.

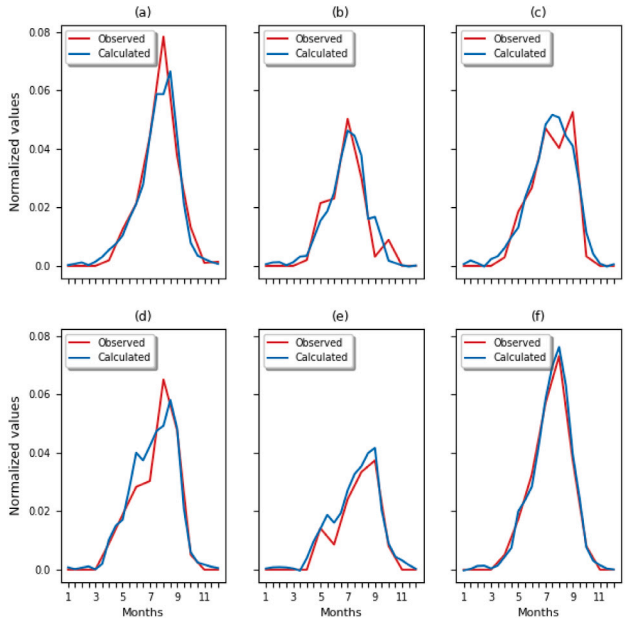

Fig. 17. Short-term forecasting — Observed and Calculated rainfall curves of the best model for test: 2015(a)–2020(f).

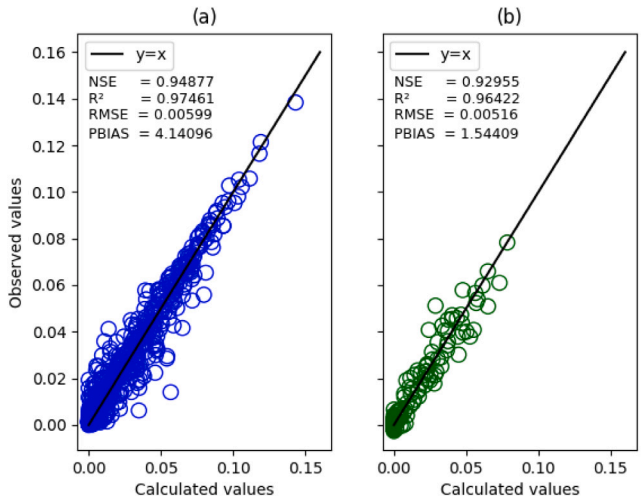

Fig. 18. Long-term forecasting — Scatter plots of the best model for training (a) and test (b).

After designing, training and testing the different models on weekly/monthly rainfall and temperature time series data, it appears that the best performing model for short-term flood forecasting is the LSTM(Stacked) model whose performance criteria are $NSE = 0.96945$, $PBIAS = 1.06640$, $R^2 = 0.98490$ and $RMSE = 0.00462$ for training, and $NSE = 0.95118$, $PBIAS = 4.74773$, $R^2 = 0.97631$ and $RMSE = 0.00429$ for test. The goodness of fit of this model is very good. For long-term flood forecasting, the best performing model is still LSTM (Stacked) with the following performance criteria: $NSE = 0.94877$, $PBIAS = 4.14095$, $R^2 = 0.97460$ and $RMSE = 0.00599$ for training, and $NSE = 0.92954$, $PBIAS = 1.54409$, $R^2 = 0.96422$ and $RMSE = 0.00516$ for test. The goodness of fit of this model is very good. The LSTM model has good flood forecasting capabilities which reflect good generalization capabilities and the absence of underfitting/overfitting during training.

The main contribution of our work is the use of ML and DL methods for short term and long term flood forecasting in the far-north region of Cameroon. Our findings are alternatives to the poorly performing physical based models used in the region. Our research can be used for the implementation of automatic flood warning systems in the Far-North region of Cameroon. They can also be used to define effective and efficient flood risk management policies to avoid or limit loss of lives and material damage, and make the Cameroon's Far-North region more resilient to flood crises. The use of ML and DL methods for real-time flood forecasting in the far north is an avenue to be explored for further work.

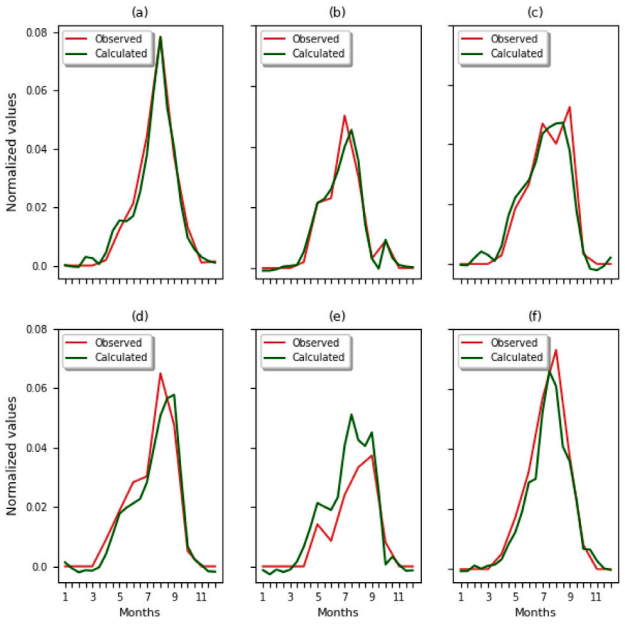

Fig. 19. Long-term forecasting — Observed and Calculated rainfall curves of the best model for test: 2015(a)–2020(f).

CRediT authorship contribution statement

Francis Yongwa Dtissibe: Conceptualization, Data curation, Formal analysis, Investigation, Methodology, Resources, Software, Writing – original draft. **Ado Adamou Abba Ari:** Conceptualization, Data curation, Formal analysis, Investigation, Methodology, Project administration, Resources, Software, Supervision, Writing – original draft, Writing – review & editing. **Hamadjam Abboubakar:** Project administration, Resources, Supervision, Writing – original draft, Writing – review & editing. **Arouna Ndam Njoya:** Data curation, Formal analysis, Investigation, Methodology, Software. **Alidou Mohamadou:** Project administration, Supervision, Writing – review & editing. **Ousmane Thiare:** Conceptualization, Methodology, Project administration, Resources, Supervision.

Declaration of competing interest

The authors declare that they have no known competing financial interests or personal relationships that could have appeared to influence the work reported in this paper.

Acknowledgment

We like to thank the editor and the anonymous reviewers for their valuable remarks that helped us in better improving the content and presentation of the paper.

References

[1] IFRC, World Disasters Report 2020 : Come Heat or High Water, Tech. rep., International Federation of Red Cross and Red Crescent Societies (IFRC), Geneva, Switzerland, 2020.
[2] F.Y. Dtissibe, A.A.A. Ari, C. Titouna, O. Thiare, A.M. Gueroui, Flood forecasting based on an artificial neural network scheme, Nat. Hazards 104 (2) (2020) 1211–1237.
[3] F. Falah, O. Rahmati, M. Rostami, E. Ahmadisharaf, I.N. Daliakopoulos, H.R. Pourghasemi, Artificial neural networks for flood susceptibility mapping in data-scarce urban areas, in: Spatial Modeling in GIS and R for Earth and Environmental Sciences, Elsevier, 2019, pp. 323–336.
[4] Y. Simonov, Latest tools and methodologies for flood modeling, 2017.
[5] UNISDR, Global Assessment Report on Disaster Risk Reduction 2022: Our World at Risk: Transforming Governance for a Resilient Future, Tech. rep., United Nations Office for Disaster Risk Reduction (UNISDR), Geneva, Switzerland, 2022.
[6] H. Tamiru, M.O. Dinka, Application of ANN and HEC-RAS model for flood inundation mapping in lower Baro Akobo River Basin, Ethiopia, J. Hydrol.: Reg. Stud. 36 (2021) 100855.
[7] C. Ofoegbu, P.W. Chirwa, Analysis of rural people's attitude towards the management of tribal forests in South Africa, J. Sustain. For. 38 (4) (2019) 396–411.
[8] GFDRR, Evaluation de l'État du Barrage, des Digues, du Réservoir et des Structures Hydrauliques du Système de Maga-Logone-Vrick. Cameroun, Tech. rep., Global Facility for Disaster Reduction and Recovery (GFDRR), 2012.

[9] O. Leumbe, D. Bitom, L. Mamdem, D. Tiki, A. Ibrahim, Cartographie des zones à risques d'inondation en zone soudano-sahélienne: cas de Maga et ses environs dans la région de l'extrême-nord Cameroun, Afr. Sci.: Rev. Int. Sci. Technol. 11 (3) (2015) 45–61.
[10] L. Bouba, S. Sauvagnargues, B. Gonne, P.-A. Ayral, A. Ombolo, Trends in rainfall and flood hazard in the Far North region of Cameroon, Geo-Eco-Trop 41 (3) (2017) 339–358.
[11] UNISDR, Global Assessment Report on Disaster Risk Reduction, Tech. rep., United Nations Office for Disaster Risk Reduction (UNISDR), Geneva, Switzerland, 2019.
[12] A. Quesada-Román, J.A. Ballesteros-Cánovas, S. Granados-Bolaños, C. Birkel, M. Stoffel, Improving regional flood risk assessment using flood frequency and dendrogeomorphic analyses in mountain catchments impacted by tropical cyclones, Geomorphology 396 (2022) 108000.
[13] IFRC, World Disasters Report 2022 : Trust, Equity and Local Action, Tech. rep., International Federation of Red Cross and Red Crescent Societies (IFRC), Geneva, Switzerland, 2023.
[14] G. Gao, Y. Li, J. Li, X. Zhou, Z. Zhou, A hybrid model for short-term rainstorm forecasting based on a back-propagation neural network and synoptic diagnosis, Atmos. Ocean. Sci. Lett. 14 (5) (2021) 100053.
[15] S. Nevo, E. Morin, A. Gerzi Rosenthal, A. Metzger, C. Barshai, D. Weitzner, D. Voloshin, F. Kratzert, G. Elidan, G. Dror, et al., Flood forecasting with machine learning models in an operational framework, Hydrol. Earth Syst. Sci. Discuss. (2021) 1–31.
[16] J. Tanzouak, I. Sarr, N. Bame, B. Yenke, S. Faye, Adjustment module to give auto-adaptiveness behavior to flood forecasting systems, in: African Conference on Research in Computer Science and Applied Mathematics(CARI), Stellenbosch, South Africa, 2018, pp. 2018–225.
[17] W.F. Krajewski, G.R. Ghimire, I. Demir, R. Mantilla, Real-time streamflow forecasting: AI vs. Hydrologic insights, J. Hydrol. X 13 (2021) 100110.
[18] A. Mosavi, P. Ozturk, K.-w. Chau, Flood prediction using machine learning models: Literature review, Water 10 (11) (2018) 1536.
[19] F. Mahmud, M. Limon, A. Khayer, S.A. Osmani, A data-driven approach to forecast floods in Sylhet city using machine learning and deep learning techniques, in: AIP Conference Proceedings, Vol. 2713, AIP Publishing, 2023.
[20] V. Atashi, R. Kardan, H.T. Gorji, Y.H. Lim, Comparative study of deep learning LSTM and 1D-CNN models for real-time flood prediction in Red River of the North, USA, in: 2023 IEEE International Conference on Electro Information Technology (eIT), IEEE, 2023, pp. 022–028.
[21] F. Ghobadi, D. Kang, Improving long-term streamflow prediction in a poorly gauged basin using geo-spatiotemporal mesoscale data and attention-based deep learning: A comparative study, J. Hydrol. 615 (2022) 128608.
[22] F. Granata, F. Di Nunno, G. de Marinis, Stacked machine learning algorithms and bidirectional long short-term memory networks for multi-step ahead streamflow forecasting: A comparative study, J. Hydrol. 613 (2022) 128431.
[23] X.-H. Le, D.-H. Nguyen, S. Jung, M. Yeon, G. Lee, Comparison of deep learning techniques for river streamflow forecasting, IEEE Access 9 (2021) 71805–71820.
[24] F. Hussain, R.-S. Wu, J.-X. Wang, Comparative study of very short-term flood forecasting using physics-based numerical model and data-driven prediction model, Nat. Hazards 107 (1) (2021) 249–284.
[25] M. Rahimzad, A. Moghaddam Nia, H. Zolfonoon, J. Soltani, A. Danandeh Mehr, H.-H. Kwon, Performance comparison of an LSTM-based deep learning model versus conventional machine learning algorithms for streamflow forecasting, Water Resour. Manag. 35 (12) (2021) 4167–4187.
[26] H.M. Idan, K.Q. Hussein, Comparison study between selected techniques of (ML, SVM and Deep Learning) regarding prediction of Flooding in Eastof Iraq, Turk. J. Comput. Math. Educ. (TURCOMAT) 12 (14) (2021) 2893–2904.
[27] N.B.M. Khairudin, N.B. Mustapha, T.N.B.M. Aris, M.B. Zolkepli, Comparison of machine learning models for rainfall forecasting, in: 2020 International Conference on Computer Science and Its Application in Agriculture (ICOSICA), IEEE, 2020, pp. 1–5.
[28] K. Ghaderi, B. Motamedvaziri, M. Vafakhah, A.A. Dehghani, Regional flood frequency modeling: a comparative study among several data-driven models, Arab. J. Geosci. 12 (18) (2019) 1–9.
[29] B. Choubin, S. Khalighi-Sigaroodi, A. Malekian, Ö. Kişi, Multiple linear regression, multi-layer perceptron network and adaptive neuro-fuzzy inference system for forecasting precipitation based on large-scale climate signals, Hydrol. Sci. J. 61 (6) (2016) 1001–1009.
[30] A. Lohani, R. Kumar, R. Singh, Hydrological time series modeling: A comparison between adaptive neuro-fuzzy, neural network and autoregressive techniques, J. Hydrol. 442 (2012) 23–35.
[31] W.-C. Wang, K.-W. Chau, C.-T. Cheng, L. Qiu, A comparison of performance of several artificial intelligence methods for forecasting monthly discharge time series, J. Hydrol. 374 (3–4) (2009) 294–306.
[32] M. Firat, Comparison of artificial intelligence techniques for river flow forecasting, Hydrol. Earth Syst. Sci. 12 (1) (2008) 123–139.
[33] M. Nayak, S. Das, M.R. Senapati, Improving flood prediction with deep learning methods, J. Inst. Eng. (India): Ser. B 103 (4) (2022) 1189–1205.
[34] Y. Tao, X. Gao, A. Ihler, K. Hsu, S. Sorooshian, Deep neural networks for precipitation estimation from remotely sensed information, in: 2016 IEEE Congress on Evolutionary Computation (CEC), IEEE, 2016, pp. 1349–1355.
[35] A. Haidar, B. Verma, Monthly rainfall forecasting using one-dimensional deep convolutional neural network, IEEE Access 6 (2018) 69053–69063.
[36] S. Kabir, S. Patidar, X. Xia, Q. Liang, J. Neal, G. Pender, A deep convolutional neural network model for rapid prediction of fluvial flood inundation, J. Hydrol. 590 (2020) 125481.
[37] S.P. Van, H.M. Le, D.V. Thanh, T.D. Dang, H.H. Loc, D.T. Anh, Deep learning convolutional neural network in rainfall–runoff modelling, J. Hydroinform. 22 (3) (2020) 541–561.
[38] C. Chen, Q. Hui, W. Xie, S. Wan, Y. Zhou, Q. Pei, Convolutional Neural Networks for forecasting flood process in Internet-of-Things enabled smart city, Comput. Netw. 186 (2021) 107744.
[39] Y.R. Sari, E.C. Djamal, F. Nugraha, Daily rainfall prediction using one dimensional convolutional neural networks, in: 2020 3rd International Conference on Computer and Informatics Engineering (IC2IE), IEEE, 2020, pp. 90–95.
[40] D. Hussain, T. Hussain, A.A. Khan, S.A.A. Naqvi, A. Jamil, A deep learning approach for hydrological time-series prediction: A case study of Gilgit river basin, Earth Sci. Inform. 13 (3) (2020) 915–927.
[41] K. Ishida, A. Ercan, T. Nagasato, M. Kiyama, M. Amagasaki, Use of 1D-CNN for input data size reduction of LSTM in Hourly Rainfall-Runoff modeling, 2021, arXiv preprint arXiv:2111.04732.
[42] I.R. Widiasari, L.E. Nugoho, R. Efendi, et al., Context-based hydrology time series data for a flood prediction model using LSTM, in: 2018 5th International Conference on Information Technology, Computer, and Electrical Engineering (ICITACEE), IEEE, 2018, pp. 385–390.
[43] X.-H. Le, H.V. Ho, G. Lee, S. Jung, Application of long short-term memory (LSTM) neural network for flood forecasting, Water 11 (7) (2019) 1387.
[44] T. Song, W. Ding, J. Wu, H. Liu, H. Zhou, J. Chu, Flash flood forecasting based on long short-term memory networks, Water 12 (1) (2019) 109.
[45] F. Kratzert, D. Klotz, C. Brenner, K. Schulz, M. Herrnegger, Rainfall–runoff modelling using long short-term memory (LSTM) networks, Hydrol. Earth Syst. Sci. 22 (11) (2018) 6005–6022.
[46] Z. Xiang, J. Yan, I. Demir, A rainfall-runoff model with LSTM-based sequence-to-sequence learning, Water Resour. Res. 56 (1) (2020) e2019WR025326.
[47] S. Haojun, L. Yong, Z. Zongci, W. Hanjie, Prediction of summer precipitation in China based on LSTM network, Prog. Clim. Change Res. 16 (3) (2020) 263–275.
[48] I.-F. Kao, Y. Zhou, L.-C. Chang, F.-J. Chang, Exploring a Long Short-Term Memory based Encoder-Decoder framework for multi-step-ahead flood forecasting, J. Hydrol. 583 (2020) 124631.
[49] X. Guo, Y. Gao, Y. Li, D. Zheng, D. Shan, Short-term household load forecasting based on Long-and Short-term Time-series network, Energy Rep. 7 (2021) 58–64.
[50] Z. Fang, Y. Wang, L. Peng, H. Hong, Predicting flood susceptibility using LSTM neural networks, J. Hydrol. 594 (2021) 125734.

[51] K.M. Hunt, G.R. Matthews, F. Pappenberger, C. Prudhomme, Using a long short-term memory (LSTM) neural network to boost river streamflow forecasts over the western United States, Hydrol. Earth Syst. Sci. Discuss. (2022) 1–30.

[52] D. Coyle, A. Weller, "Explaining" machine learning reveals policy challenges, Science 368 (6498) (2020) 1433–1434.

[53] S. Lek, I. Dimopoulos, M. Derraz, Y. El Ghachtoul, Modélisation de la relation pluie-débit à l'aide des réseaux de neurones artificiels, Rev. Sci. eau/J. Water Sci. 9 (3) (1996) 319–331.

[54] S. Riad, J. Mania, L. Bouchaou, Y. Najjar, Rainfall-runoff model usingan artificial neural network approach, Math. Comput. Modelling 40 (7–8) (2004) 839–846.

[55] M.S. Toukourou, A. Johannet, G. Dreyfus, Flash flood forecasting by statistical learning in the absence of rainfall forecast: a case study, in: International Conference on Engineering Applications of Neural Networks, Springer, 2009, pp. 98–107.

[56] D. Llamas Gaspar, Application de l'apprentissage artificiel à la modélisation systémique de la chaîne hydrométéorologique pour la prévision des crues éclair, 2010.

[57] A. Bornancin-Plantier, A. Johannet, P. Roussel-Ragot, G. Dreyfus, Flash flood forecasting using neural networks without rainfall forecasts: model selection and generalization capability geophysical research abstracts, 2011, EGU2011–1794.

[58] S.H. Elsafi, Artificial neural networks (ANNs) for flood forecasting at Dongola Station in the River Nile, Sudan, Alex. Eng. J. 53 (3) (2014) 655–662.

[59] O. Kharroubi, O. Blanpain, E. Masson, S. Lallahem, Application du réseau des neurones artificiels à la prévision des débits horaires: Cas du bassin versant de l'eure, france, Hydrol. Sci. J. 61 (3) (2016) 541–550.

[60] G. Artigue, A. Johannet, V. Borell, S. Pistre, Neural network flash flood forecasting: generalizing to ungauged basins, in: Geophysical Research Abstracts, Vol. 21, 2019.

[61] B.D. Bowes, J.M. Sadler, M.M. Morsy, M. Behl, J.L. Goodall, Forecasting groundwater table in a flood prone coastal city with long short-term memory and recurrent neural networks, Water 11 (5) (2019) 1098.

[62] C.K. Sønderby, L. Espeholt, J. Heek, M. Dehghani, A. Oliver, T. Salimans, S. Agrawal, J. Hickey, N. Kalchbrenner, Metnet: A neural weather model for precipitation forecasting, 2020, arXiv preprint arXiv:2003.12140.

[63] L. Zhihua, J. Zuo, D. Rodriguez, Predicting of runoff using an optimized SWAT-ANN: a case study, J. Hydrol.: Reg. Stud. 29 (2020) 100688.

[64] T. Naili, A. Louazene, Détection De Visage Par Un Modèle CNN (Ph.D. thesis), UNIVERSITY OF OUARGLA.

[65] S. Ghimire, Z.M. Yaseen, A.A. Farooque, R.C. Deo, J. Zhang, X. Tao, Streamflow prediction using an integrated methodology based on convolutional neural network and long short-term memory networks, Sci. Rep. 11 (1) (2021) 1–26.

[66] T. Liu, H. Xu, M. Ragulskis, M. Cao, W. Ostachowicz, A data-driven damage identification framework based on transmissibility function datasets and one-dimensional convolutional neural networks: verification on a structural health monitoring benchmark structure, Sensors 20 (4) (2020) 1059.

[67] S. Hochreiter, J. Schmidhuber, Long short-term memory, Neural Comput. 9 (8) (1997) 1735–1780.

[68] C. Hu, Q. Wu, H. Li, S. Jian, N. Li, Z. Lou, Deep learning with a long short-term memory networks approach for rainfall-runoff simulation, Water 10 (11) (2018) 1543.

[69] W. Li, X. Gao, Z. Hao, R. Sun, Using deep learning for precipitation forecasting based on spatio-temporal information: a case study, Clim. Dynam. 58 (1) (2022) 443–457.

[70] Q. Zhang, J. Zhang, J. Zou, S. Fan, A novel fault diagnosis method based on stacked lstm, IFAC-PapersOnLine 53 (2) (2020) 790–795.

[71] Y. Li, H. Xu, M. Bian, J. Xiao, Attention based CNN-ConvLSTM for pedestrian attribute recognition, Sensors 20 (3) (2020) 811.

[72] H. Tamiru, M. Wagari, Evaluation of data-driven model and GIS technique performance for identification of Groundwater Potential Zones: A case of Fincha Catchment, Abay Basin, Ethiopia, J. Hydrol.: Reg. Stud. 37 (2021) 100902.

[73] K.-I. Funahashi, On the approximate realization of continuous mappings by neural networks, Neural Netw. 2 (3) (1989) 183–192.

[74] G. Cybenko, Approximation by superpositions of a sigmoidal function, Math. Control Signals Systems 5 (4) (1992) 455.

[75] A.R. Barron, Universal approximation bounds for superpositions of a sigmoidal function, IEEE Trans. Inform. Theory 39 (3) (1993) 930–945.

[76] Q. Zhang, J. Zhang, Z. Chen, M. Zhang, S. Li, A stock decision model based on optimized neural network algorithm, in: Fuzzy Systems and Data Mining V, IOS Press, 2019, pp. 523–533.

[77] K.G. Sheela, S.N. Deepa, Review on methods to fix number of hidden neurons in neural networks, Math. Probl. Eng. 2013 (2013).

[78] A. Cheo, Understanding seasonal trend of rainfall for the better planning of water harvesting facilities in the Far-North region, Cameroon, Water Util. J. 13 (2016) 3–11.

[79] ONACC, Pluviométrie et Température dans la Région de l'Extrême-Nord Cameroun : Analyse de l'Évolution de 1950 à 2015 et Projections Jusqu'à l'Horizon 2090, Tech. rep., Observatoire National sur les Changements Climatiques (ONACC), Yaoundé, Cameroun, 2018.

[80] A.E. Cheo, H.-J. Voigt, F. Wendland, Modeling groundwater recharge through rainfall in the far-north region of Cameroon, Groundw. Sustain. Dev. 5 (2017) 118–130.

[81] G.R. Ghimire, W.F. Krajewski, T.B. Ayalew, R. Goska, Hydrologic investigations of radar-rainfall error propagation to rainfall-runoff model hydrographs, Adv. Water Resour. 161 (2022) 104145.

[82] M. Fofana, J. Adounkpe, I. Larbi, J. Hounkpe, H.D. Koubodana, A. Toure, H.B. Maiga, S.-Q. Dotse, A.M. Limantol, Urban flash flood and extreme rainfall events trend analysis in Bamako, Mali, Environ. Chall. (2022) 100449.

[83] M.-T. Sattari, A. Rezazadeh-Joudi, A. Kusiak, Assessment of different methods for estimation of missing data in precipitation studies, Hydrol. Res. 48 (4) (2017) 1032–1044.

[84] A. Faruq, A. Marto, N.K. Izzaty, A.T. Kuye, S.F.M. Hussein, S.S. Abdullah, Flood disaster and early warning: application of ANFIS for river water level forecasting, Kinet.: Game Technol. Inf. Syst. Comput. Netw. Comput. Electron. Control (2021) 1–10.

[85] D. Ouali, A. Cannon, Estimation of rainfall intensity–duration–frequency curves at ungauged locations using quantile regression methods, Stoch. Environ. Res. Risk Assess. 32 (10) (2018) 2821–2836.

[86] J. Pérez-Sánchez, J. Senent-Aparicio, F. Segura-Méndez, D. Pulido-Velazquez, R. Srinivasan, Evaluating hydrological models for deriving water resources in peninsular Spain, Sustainability 11 (10) (2019) 2872.

[87] Y. Wang, R. Liu, L. Guo, J. Tian, X. Zhang, L. Ding, C. Wang, Y. Shang, Forecasting and providing warnings of flash floods for ungauged mountainous areas based on a distributed hydrological model, Water 9 (10) (2017) 776.